SUPPORTING INFORMATION

S1. Calculation of the logarithmic resource gradients

In this section we provide analytic estimates for the light and nutrient gradients resulting from a single species population in the phytoplankton model, eqns 3–6. We calculate resource distributions in the production layer, defined by the critical depths z_N^* and z_I^* where either the nutrient or the light intensity reaches a critical value, $N(z_N^*) = N^*$ and $I(z_I^*) = I^*$ (see dashed lines in Figs. 2b and c). We further assume small mortality $m \ll \mu_{max}$, so that the biomass can diffuse from the favorable layer without essential losses and the phytoplankton density has only small variation within the favorable layer, i.e. $P(z) \approx P_0$ for $z_N^* \leq z \leq z_I^*$.

From eqn 6 within the favorable range the logarithmic gradient of the light intensity equals

$$c_I = -\frac{d \ln I(z)}{dz} = K_{bg} + kP_0, \tag{S1}$$

and the light distribution can be written

$$I(z) = I^* e^{c_I (z_I^* - z)} \ . \tag{S2}$$

Regarding the nutrient profile we assume that for small mortality the critical nutrient concentrations are small, $N^* \ll H_N$, so that the growth rate close to the critical point $N \approx N^*$ can be linearized $\mu_N(N) \approx \mu_{max} \frac{N}{H_N}$. Substituting this expression into eqn 5 we obtain at equilibrium

$$-\alpha \mu_{max} \frac{N}{H_N} P_0 + D \frac{dN}{dz^2} = 0 \ .$$

A solution to this equation, that is monotonically increasing with depth, is given by

$$N(z) = N^* e^{c_N (z - z_N^*)} \ , \tag{S3}$$

with the logarithmic gradient

$$c_N = \frac{d \ln N(z)}{dz} = \sqrt{\frac{\alpha \mu_{max} P_0}{D H_N}} \ . \tag{S4}$$

To complete our calculation the phytoplankton density in the production layer is estimated as $P_0 \sim \frac{B}{w}$ where B is the total biomass and the width of the production layer $w = |z_N^* - z_I^*|$ only weakly depends on the model parameters (Beckmann and Hense 2007). If the biomass maximum is located far from the surface, the value of B can be estimated in two limiting cases (Klausmeier and Litchman 2001)

$$B = \begin{cases} \frac{\ln(I_{in}/I^*)}{k} & \text{if } P_0 k \gg K_{bg} \\ \frac{D(N_B - N^*)}{\alpha m Z_M} & \text{if } P_0 k \ll K_{bg} \end{cases} \tag{S5}$$

where $Z_M = Z_B - \ln(I_{in}/I^*)/K_{bg}$.

These equations can be further simplified because typically $N_B \gg N^*$. Substituting eqns S5 into eqns S1 and S4, we obtain the ratio of resource gradients $\gamma = c_I/c_N$ (see also Fig. S2)

$$\gamma = \begin{cases} \dfrac{K_{bg} + \dfrac{\ln(I_{in}/I^*)}{w}}{\sqrt{\dfrac{\alpha}{k}\dfrac{\mu_{max}}{DH_N}\dfrac{\ln(I_{in}/I^*)}{w}}} & \text{if } P_0 k \gg K_{bg} \\ \dfrac{K_{bg} + \dfrac{k}{\alpha}\dfrac{DN_B}{wmZ_M}}{\sqrt{\dfrac{\mu_{max}}{H_N}\dfrac{N_B}{wmZ_M}}} & \text{if } P_0 k \ll K_{bg}. \end{cases} \tag{S6}$$

S2. Bifurcation lines in Fig. 5

In this section we derive analytic estimates for combinations of critical resource values that allow mutual invasibility of a fixed "reference" species 1 with a variable "test" species 2 (bifurcation lines in Fig. 5a main text). Both species differ in the values of consumption rates, k_i and α_i, have identical maximal growth rate μ_{max} and mortality m, but while the critical resource values N_1^* and I_1^* of the reference species are fixed, N_2^* and I_2^* are taken from a wide range.

The critical resource values of all test species that can invade in the presence of the reference species are determined by the invasibility criterion, eqn 12

$$\frac{1}{c_{N,1}} \ln \frac{N_2^*}{N_1^*} + \frac{1}{c_{I,1}} \ln \frac{I_2^*}{I_1^*} < 0 \ . \tag{S7}$$

The border of this region is shown as a green dashed line in Fig. 5a. Similar, we obtain the critical resource values of the test species, which allow the invasion of the reference species when the test species has reached equilibrium

$$\frac{1}{c_{N,2}} \ln \frac{N_1^*}{N_2^*} + \frac{1}{c_{I,2}} \ln \frac{I_1^*}{I_2^*} < 0 \ . \tag{S8}$$

In this case however, to plot the bifurcation line, we need to consider the dependence of $c_{N,2}$ and $c_{I,2}$ on the critical resource values, N_2^* and I_2^*, of the test species (see. eqns S1, S4 and S5). For these aims we pick first one special "hybrid" test species, that has the same critical resource values N_1^*, I_1^* as the reference species, but consumption rates, α_2 and k_2. We denote the logarithmic resources gradients of this species as $c'_{N,2}$ and $c'_{I,2}$.

To proceed we assume that the critical resource values are small: assuming $N_i^* \ll N_B$ we approximate $N_B - N_2^* \approx N_B$, and assuming $I_i^* \ll I_{in}$ we obtain

$$\ln \frac{I_{in}}{I_2^*} \approx \ln \frac{I_{in}}{I_1^*} - O\left(\frac{I_2^* - I_1^*}{I_{in}}\right) \ .$$

Thus, in both limits, $K_{bg} \gg P_0 k$ and $K_{bg} \ll P_0 k$, in eqn S5 the total biomass B, and from eqn S1 also the value of $c_{I,2}$, is independent of the critical resource values N_2^*, I_2^* of the test species. This means that the logarithmic light gradients are identical for all test species

$$c_{I,2} = c'_{I,2} \ .$$

In a similar way we estimate the logarithmic nutrient gradients, but from eqn S4 the value of $c_{N,2}$ depends on the half-saturation constant of the test species, $c_{N,2} \sim \sqrt{1/H_{N,2}}$. Then the logarithmic nutrient gradient of an arbitrary test species can be expressed in terms of the logarithmic nutrient gradient of the "hybrid" species

$$c_{N,2} = c'_{N,2} \sqrt{\frac{H_{N,1}}{H_{N,2}}},$$

and using the identity $H_{N,1}/H_{N,2} = N_1^*/N_2^*$ we obtain

$$c_{N,2} = c'_{N,2} \sqrt{\frac{N_1^*}{N_2^*}}.$$

Therefore, inequality S8 takes the form

$$\frac{1}{c'_{N,2}} \sqrt{\frac{N_2^*}{N_1^*}} \ln \frac{N_2^*}{N_1^*} + \frac{1}{c'_{I,2}} \ln \frac{I_2^*}{I_1^*} > 0 \ , \tag{S9}$$

where the parameters $c'_{N,2}$ and $c'_{I,2}$ are calculated for the "hybrid" species having the critical resource values, N_1^* and I_1^*, and the consumption rates, k_2 and α_2. Note that this expression holds in both limits when $K_{bg} \gg P_0 k$ and when $K_{bg} \ll P_0 k$, implying that it might provide a good approximation in general. The border of this region is shown as red dashed line in Fig. 5a.

S3. Invasion thresholds and principal eigenvalues

The dynamics of a spatially extended population $P(z,t)$ is determined by a reaction-diffusion equation, eqn 4, with certain boundary conditions. The solution to this equation can be presented in the form

$$P(z,t) = \sum_{n=1}^{\infty} e^{\lambda_n t} \psi_n(z) \ , \tag{S10}$$

where ψ_n and λ_n are the eigenfunctions and eigenvalues of the equation

$$(\mu(z) - m - \lambda_n)\psi_n + D\frac{d\psi(z)}{dz^2} = 0 \tag{S11}$$

with the same boundary conditions for the functions $\psi_n(z)$. The eigenvalue λ^* with the largest real part, the so-called principal eigenvalue, is of special interest for determining the dynamics of $P(z,t)$ because the term with this eigenvalue dominates the sum S10 at large times (see e.g., Ryabov & Blasius 2008). The sign of the real part of the principal eigenvalue determines if the population will grow, and so is able to persist $\lambda^* > 0$, or if it declines exponentially on the whole habitat, $\lambda^* < 0$. Note, that λ^* depends on the spatial resource profiles and therefore may change in time with depletion of resources by a growing population. If a species has attained equilibrium, it has zero population net growth and its principal eigenvalue equals zero, $\lambda^* = 0$.

The principal eigenvalue can be used for invasion analysis in a spatially extended system. We can define a family of invaders which for small initial density in the presence of the resident species have zero net growth, and thus a zero principal eigenvalue $\lambda^*_{inv} = 0$. In the space of the invader's critical resource values, this family defines the invasion threshold (in general, a hypersurface), separating successful and unsuccessful invaders. In our setting, and given that resident and invader have identical maximal growth rate, $\mu_{\max,2} = \mu_{\max,1}$, and mortality, $m_2 = m_1$, this corresponds to the condition $\Delta = c_{N,1}^{-1} \ln H_{N,2}/H_{N,1} + c_{I,1}^{-1} \ln H_{I,2}/H_{I,1} = 0$ (see eqn 11).

Now consider an invader which has the same half saturation constants as the resident species, but different maximal growth rate, $\mu_{\max,2}$, mortality, m_2, or dispersal ability, D_2. It can be shown (Stakgold, 2000) that the eigenvalue spectrum, and in particular the principal eigenvalue, of this species shifts in the positive direction with an increase of the growth rate difference $\mu_{max,2} - \mu_{max,1}$, and in the negative direction with an increase in the difference of destructive factors, such as dispersal rates $D_2 - D_1$ or mortalities $m_2 - m_1$. Thus, in general, the invader's principal eigenvalue will be positive or negative, even though the constant remains $\Delta = 0$ (since the half saturation constants remain unchanged). Assume without loss of generality that the invader has a positive total growth rate, $\lambda^*_{inv} > 0$. This means that it should be possible to invade the system with even higher resource requirements. Thus, there should be a 'border-line' invader with the same values of $\mu_{\max,2}$, m_2, and D_2, but larger half saturation constants so that its principal eigenvalue equals zero, $\lambda^*_{inv} = 0$. As the resource requirements of this second invader are higher, its Δ value is positive. This value, which we denote by Δ^*_{12}, defines the difference in the favorable ranges (according to eqn 11) between this species and the resident. Thus all species with maximal growth rate $\mu_{\max,2}$, dispersal rate D_2 and mortality m_2, and whose half-saturation constants satisfy the inequality

$$\frac{1}{c_{N,1}} \ln \frac{H_{N,2}}{H_{N,1}} + \frac{1}{c_{I,1}} \ln \frac{H_{I,2}}{H_{I,1}} < \Delta^*_{12} \tag{S12}$$

can invade the system. As the boundary problem can not be solved in general, we cannot calculate the value of Δ^*_{12} but we can make some predictions about its sign. Similar to λ^*_{inv}, this value increases with $(\mu_{max,2} - \mu_{max,1})$, decreases with $m_2 - m_1$ and $D_2 - D_1$, equals zero when all these differences vanish, and changes sign together with λ^*_{inv}.

Assuming Monod limitation of growth by two essential resources (eqn 3) we can rewrite eqn S12 in terms of the critical resources values

$$\frac{1}{c_{N,1}} \ln \frac{N^*_2}{N^*_1} + \frac{1}{c_{I,1}} \ln \frac{I^*_2}{I^*_1} < \Delta_{12} \ , \tag{S13}$$

where

$$\Delta_{12} = \Delta^*_{12} + \left(\frac{1}{c_{N,1}} + \frac{1}{c_{I,1}} \right) \ln \frac{(\mu_{\max,1} - m_1) m_2}{(\mu_{\max,2} - m_2) m_1} \ . \tag{S14}$$

Eqns. S13 and S14 define the invasion threshold for the invader, species 2, as a straight line with slope $\gamma_1 = c_{N,1}/c_{I,1}$ in double logarithmic resource space. The location of the invasion threshold depends in a complex way on the resource gradients and on the differences in maximal growth rate, $\mu_{\max,i}$, mortality, m_i, or dispersal rates, D_i. In the resource plane, the invasion threshold can be located above ($\Delta_{12} > 0$) or below ($\Delta_{12} < 0$) the critical resource values of the resident, (N^*_1, I^*_1), see Fig 4a.

Consider a special case when the growth and mortality rates of species 2 are rescaled, $\mu_{\max,2} = \beta \mu_{\max,1}$ and $m_2 = \beta m_1$. Then the second term in eqn S14 vanishes, however Δ^*_{12} can be nonzero because both $\mu_{max,2} - \mu_{max,1}$ and $m_2 - m_1$ are positive. Substituting $\mu_{\max,2}$ and m_2 into eqn 4 and dividing it by β, we obtain that in equilibrium the distribution of species 2 should satisfy the equation

$$\mu_1(z) P_2 - m_1 P_2 + \frac{D_1}{\beta} \frac{\partial^2 P_2}{\partial z^2} = 0 \ .$$

Therefore these changes can be interpreted as a reduction of the diffusivity $D_2 = D_1/\beta$. Since Δ^*_{12} decreases with $(D_2 - D_1)$ the shift of the invasibility threshold is positive ($\Delta^*_{12} > 0$) if $\beta > 1$ and negative ($\Delta^*_{12} < 0$) if $\beta < 1$.

S4. Extension to systems with sinking or advection

The dynamics of a population living in a unidirectional flow (e.g. sinking, floating, etc.) can be described by the reaction-diffusion-advection equation (Murray 2002, Ryabov & Blasius 2008)

$$\frac{\partial P}{\partial t} = (\mu(z) - m)P - v\frac{\partial P}{\partial z} + D\frac{\partial^2 P}{\partial z^2} \ , \tag{S15}$$

where v is the flow or sinking velocity, which is positive when the flow is directed towards larger z values. Substituting $P = \tilde{P}\exp(vz/2D)$ into eqn S15, we obtain

$$\frac{\partial \tilde{P}}{\partial t} = \mu\tilde{P} - \left(m + \frac{v^2}{4D}\right)\tilde{P} + D\frac{\partial^2 \tilde{P}}{\partial z^2} \ . \tag{S16}$$

Note that $\partial_t \tilde{P}$ has the same sign as $\partial_t P$, so that both functions grow and decline simultaneously. Furthermore, they have the same boundary conditions $\tilde{P}(0) = \tilde{P}(Z_B) = 0$. Eqn. S16 describes a population $\tilde{P}(z,t)$ in a system without flow but with an effective mortality

$$m' = m + \frac{v^2}{4D} \ . \tag{S17}$$

Therefore, the presence of an advective flow which washes out a population from a favorable range can be interpreted as an effective increase of the mortality by the value $v^2/4D$.

This higher mortality entails an increase of resource requirements. Assuming eqn 3 for the growth rate, we obtain new critical resource values

$$I_i'^* = H_{I,i}\frac{m_i'}{\mu_{max,i} - m_i'} \ , \qquad N_i'^* = H_{N,i}\frac{m_i'}{\mu_{max,i} - m_i'} \ . \tag{S18}$$

Since $m' > m$, the new critical resources values I'^* and N'^* in the presence of a positive flow are larger than in a system without flow. This, in turn shifts the zero net growth isoclines and invasion thresholds towards higher resource values in the resource plane.

S5. Model details and parameters used for figures

Numerical scheme The model was integrated using a backward difference method, based on the finite volume scheme (Pham Thi et al. 2005). For the numerical solution we have discretized all variables on a grid which consisted of 400 points. Diffusion terms were approximated by a second order central discretization scheme and integration was made via the trapezoidal rule. The resulting system of ordinary differential equations was solved by the CVODE package (http://www.netlib.org/ode). Further we verified that the results remain unchanged if we double the number of points in the grid. See Ryabov et al. (2010) for further details on numerical procedures.

Boundary conditions As boundary conditions we assumed impenetrable borders at the surface and at the bottom for the phytoplankton biomass and an impenetrable surface and a constant concentration N_B at the bottom for the nutrient.

Initial conditions We used a linear initial nutrient distribution changing from 0 at the surface to N_B at the bottom. For both phytoplankton species we assigned a uniform distribution of small initial density. We also investigated the influence of different initial conditions, however we did not find any new solutions beside the ones described.
To perform the invasion analysis, in the numerics the growth of the invader species was suppressed during the first 10000 simulation days, to make sure that an equilibrium distribution of the resident species was established. Then we simulated the system for a duration of further 40000 days to obtain the final competition outcome. To test for bistability, this simulation was repeated by a second simulation in which the roles of invader and resident were exchanged.

Parameter values Default species and model parameters are listed in Table S1.

Figure 1d. Calculation of the invasion threshold is based on 7000 simulations of invasion by species with different half saturation constants H_N and H_I. However residents and invaders have the same $\mu_{\max}$, m, and D, so that the invasion threshold is not shifted with respect to the resident (N^*, I^*) values.
Figure 2. Half-saturation constants of the invader, $H_I^{\text{inv}} = 8$ μmol photons m^{-2} and H_N^{inv} =0.09 mmol nutrient m^{-3}.
Figure 3b. The figure shows the results of more than 1000 simulations where parameter values of environmental conditions (I_{in}, K_{bg}, D, N_B) and values of consumption rates, k_i and α_i, were randomly chosen from a uniform distribution in a wide range (see Table S1). Specific parameters, which do not vary, correspond to species 1 and 2 in Table S1. In particular, the half-saturation constants, maximal growth and mortality rates were fixed, so that the critical values, $(N_i^*,\ I_i^*)$, and γ_{cr} remain constant. To determine γ_1 and γ_2 numerically we performed simulations for each species in monoculture. Typically a change in environmental parameters leads to a simultaneous increase or decrease of γ_1 and γ_2. As a result all data points group along one diagonal.
In the case of competitive dominance (where one species wins and the other is excluded) the ratio $\rho = \ln B_1/B_2$ practically approaches positive or negative infinity after our standardized simulation period of 40000 days (see above). To visualize intermediate values of ρ close to the coexistence region, the color scale was truncated at absolute values of $|\rho\,| \geq 7$, i.e. log-ratios above 7 where set to $\rho = 7$ and log-ratios below -7 where set to $\rho = -7$.
To judge bistability, simulations were repeated two times, with either species 1 taken as resident and species 2 as invader (upward-pointing triangles) or species 2 as resident and species 1 as invader (downward-pointing triangles).
Figure 5. Invasion thresholds are plotted on the basis of invasion analysis for 7000 combinations of species 1 and

test species 2. Parameter values taken as in Table S1. However, for species 2 half saturation constants were varied to achieve the chosen values of critical resources, and maximal growth rate and mortality taken as (a) $\mu_{\max,2} = 0.04$ h^{-1} and $m_2 = 0.01$ h^{-1} and (b) $\mu_{\max,2} = 0.08$ h^{-1} and $m_2 = 0.02$ h^{-1}.

References

Arndt, S., Brumsack, H.-J. & Wirtz, K.W. (2006). Cretaceous black shales as active bioreactors: A biogeochemical model for the deep biosphere encountered during ODP Leg 207 (Demerara Rise). *Geochimica et Cosmochimica Acta*, 70, 408-425.

Beckmann, A. & Hense, I. (2007). Beneath the surface: Characteristics of oceanic ecosystems under weak mixing conditions - A theoretical investigation. *Prog. Oceanogr.*, 75, 771-796.

D'Hondt, S., Jorgensen, B.B., Miller, D.J., Batzke, A., Blake, R., Cragg, B.A. et al. (2004). Distributions of Microbial Activities in Deep Subseafloor Sediments. *Science*, 306, 2216-2221.

Karl, D.M. & Letelier, R.M. (2008). Nitrogen fixation-enhanced carbon sequestration in low nitrate, low chlorophyll seascapes. *Mar. Ecol. Prog. Ser.*, 364, 257-268.

Karl, D. (2010). Oceanic ecosystem time-series programs. *Oceanography*, 23, 104.

Klausmeier, C. & Litchman, E. (2001). Algal games: The vertical distribution of phytoplankton in poorly mixed water columns. *Limnol. Oceanogr.*, 46, 1998-2007.

Litchman, E., Klausmeier, C.A., Schofield, O.M. & Falkowski, P.G. (2007). The role of functional traits and trade-offs in structuring phytoplankton communities: scaling from cellular to ecosystem level. *Ecol. Lett.*, 10, 1170-1181.

Murray, J.D. (2002) *Mathematical biology: an introduction.* Springer Verlag.

Pham Thi, N.N., Huisman, J., & Sommeijer, B.P. (2005). Simulation of three-dimensional phytoplankton dynamics: competition in light-limited environments. *Journal of Computational and Applied Mathematics*, 174, 83-96.

Ryabov, A.B. & Blasius, B. (2008). Population growth and persistence in a heterogeneous environment: the role of diffusion and advection. *Math. Model. Nat. Phenom.*, 3, 42-86.

Ryabov, A.B., Rudolf, L. & Blasius, B. (2010). Vertical distribution and composition of phytoplankton under the influence of an upper mixed layer. *J. Theor. Biol.*, 263, 120-133.

Shipboard Scientific Party (2003) Leg 201 Summary. In: *Proceedings of the Ocean Drilling Program, Initial Reports* 201, 1–81. College Station TX.

Shipboard Scientific Party (2004) Leg 207 summary. In: *Proceedings of the Ocean Drilling Program, Initial Reports* 207, 1–89. College Station TX.

Stakgold, I. (2000). *Boundary value problems of mathematical physics.* SIAM.

Torres, M.E., Brumsack, H.J., Bohrmann, G. & Emeis, K.C. (1996) Barite fronts in continental margin sediments: A new look at barium remobilization in the zone of sulfate reduction and formation of heavy barites in diagenetic fronts. *Chemical Geology*, 127, 125-139.

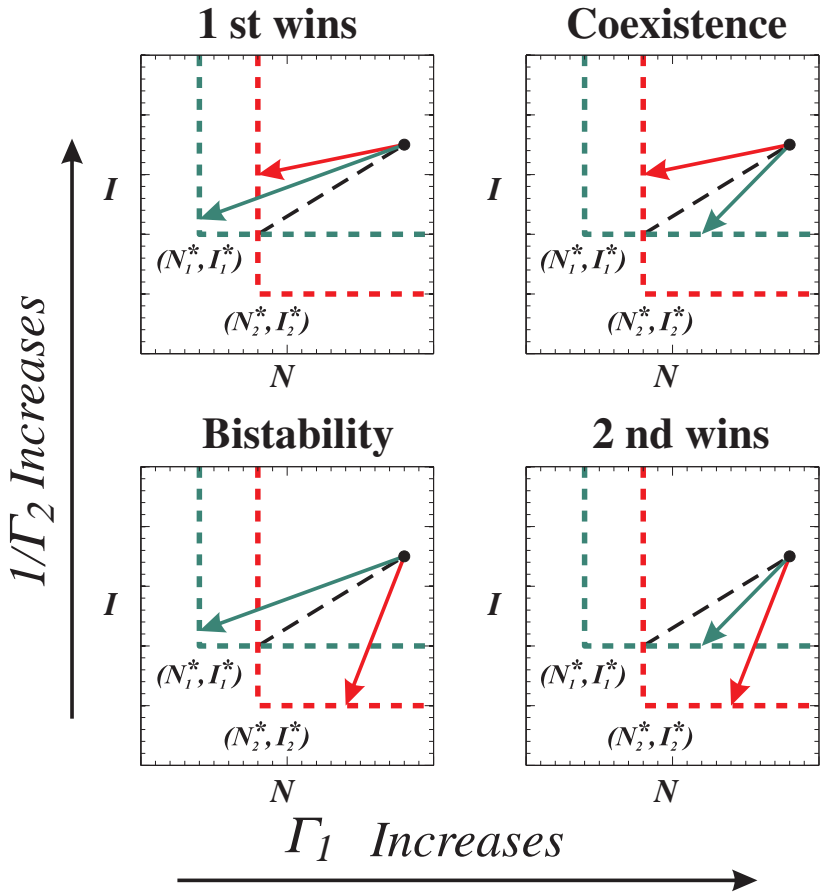

Figure S1: Two-species resource competition in a uniform system (compare to Fig. 3). The four typical cases for the competition outcome are shown, depending on the mutual slopes of consumption vectors Γ_i (values of critical resources and supply points remain fixed). For each case the zero-net-growth isoclines (ZNGI's, dashed lines) of species 1 (green) and species 2 (red) are plotted in the (N, I)-resource plane, together with the supply point (black circle) and the consumption vectors (green and red arrows). Each species in monoculture reduces resources to an equilibrium point, corresponding to the intersection of its consumption vector with its ZNGI. Invasion of the other species is possible if its critical resource values are located below this point (see Fig. 1b). Define the critical slope Γ_{cr} by the slope of a straight line from the supply point to the intersection of the two ZNGIs (indicated as black dashed line). Species 1 can invade if the consumption vector of species 2 has a slope less than the critical slope ($1/\Gamma_2 > 1/\Gamma_{cr}$, top panel), i.e. species 2 has relatively stronger influence on its most limiting resource N than on resource I. In contrast, species 2 can invade if the slope of the consumption vector of species 1 is larger than the critical slope ($\Gamma_1 > \Gamma_{cr}$, right-hand panel), i.e. species 1 has a relatively stronger influence on its most limiting resource I.

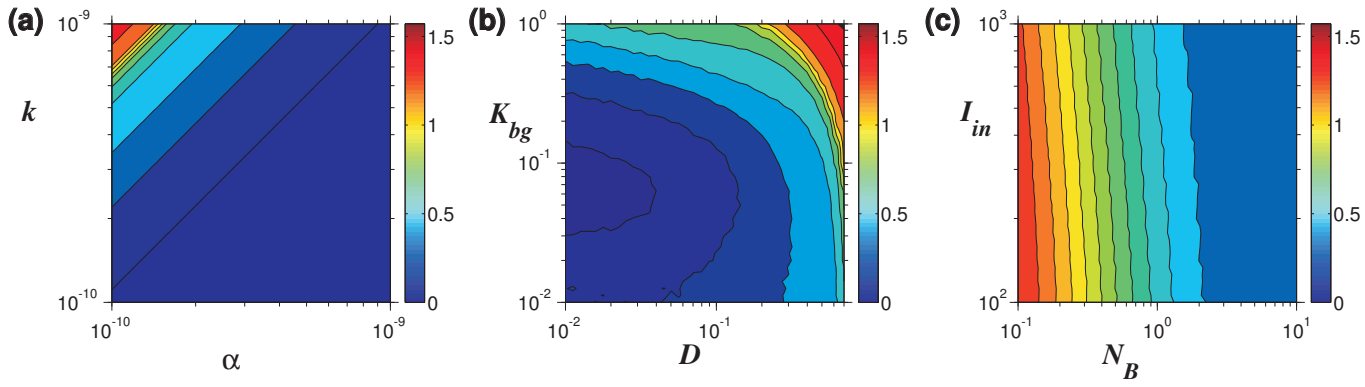

Figure S2: Ratio of the logarithmic resource gradients $\gamma_1 = c_{I,1}/c_{N,1}$ in the phytoplankton model as a function of several species specific and environmental parameters. Colorcode indicates the value of $\arctan\gamma_1$ calculated numerically for a monoculture of species 1 in the phytoplankton model (see Table S1 for parameters which do not vary). Since γ_i equals the slope of the invasion line in the resource plane, this allows to project shifts in the species composition and to gain insight of how a change of one parameter can compensate for the influence of other parameters. For example, an increase of γ corresponds to a clockwise rotation of the invasion threshold lines, thereby favoring the best nutrient competitor.

(a) Dependence of γ on species traits. Slope of the invasion threshold γ grows with the ratio k/α. This dependence is also evident from both limits in eqn S6. Together with Fig. 3, this result confirms our suggestion that two-species coexistence is more probable if each species relatively less consumes its most limiting resource (see main text).

(b) Dependence of γ on environmental conditions. Slope of the invasion threshold γ grows with turbulent diffusivity D and background turbidity K_{bg}. This indicates that a turbid but weakly-mixed environment should result in the same species composition as stronger mixed but clean waters (while the total biomass will, of course, in general be different).

(c) Dependence of γ on resource supply. Increase of incident light intensity I_{in} or of bottom nutrient concentration N_B decreases γ (thus leading to a counter-clockwise rotation of the invasion thresholds) and creates more favorable conditions for the best light competitor (compare to Fig. S3).

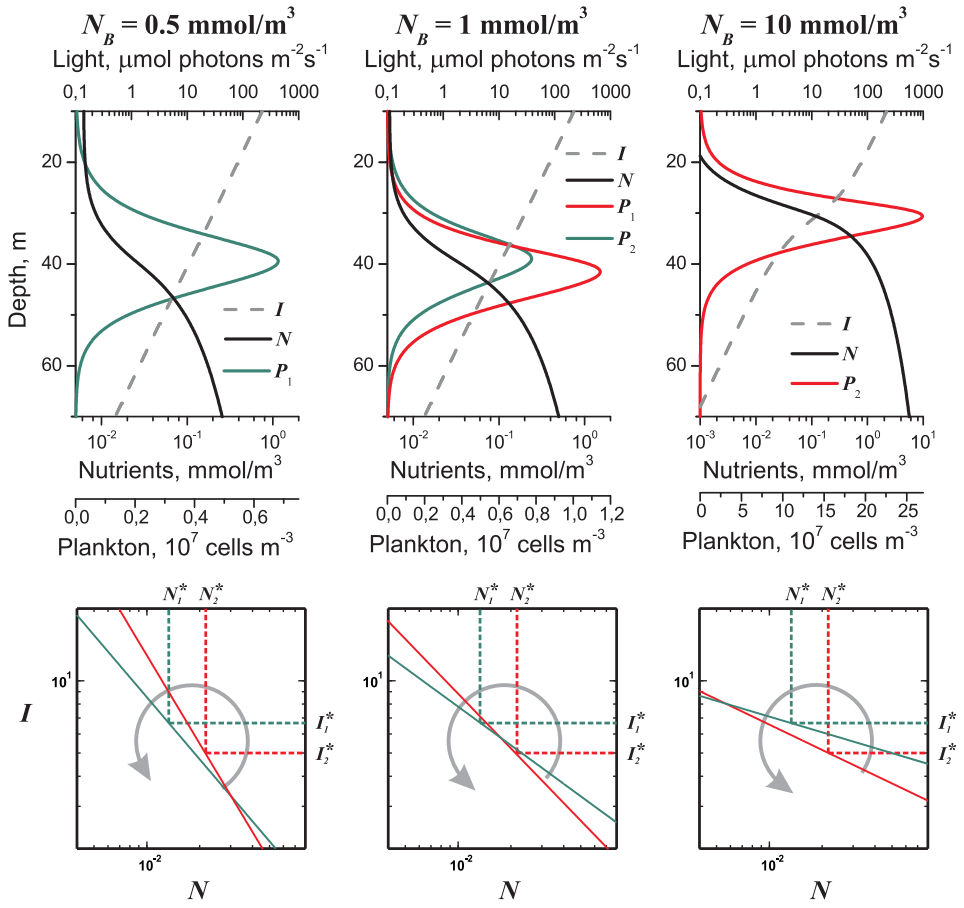

Figure S3: Geometrical method to project the outcome of spatial resource competition in dependence of the ambient nutrient concentration, N_B. Top panel: shift in the competition outcome between species 1 (green) and species 2 (red) in the phytoplankton model caused by an increase of the bottom nutrient concentration, N_B. Bottom panel illustrates this shift as the result of a counter-clockwise rotation of the invasion thresholds. The slopes, γ_1 and γ_2, of the invasion thresholds in the bottom panel were calculated numerically for a monoculture of species 1 and 2. To obtain a relatively small difference between γ_1 and γ_2 we used $\alpha_1 = 8 \times 10^{-10}$ mmol nutrient cell^{-1} and $k_2 = 6{\times}10^{-10}$ m^2 cell^{-1}.

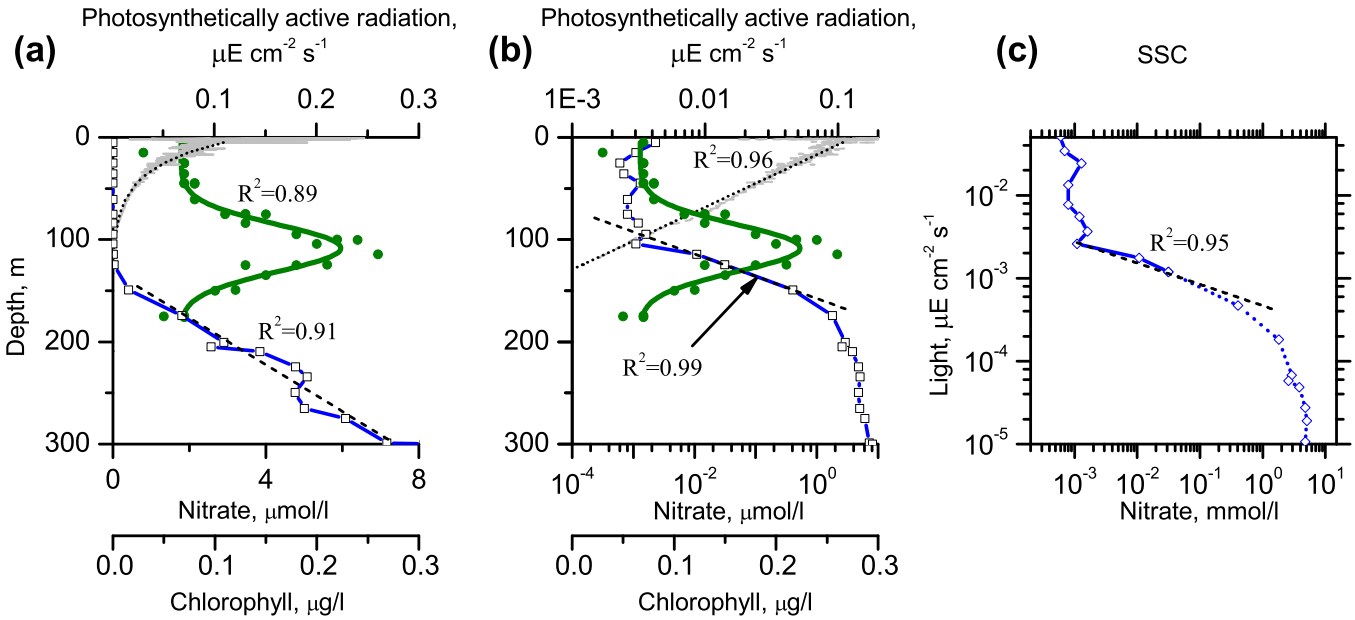

Figure S4: Exponential resource distributions in a vertical water column. Shown are the profiles of photosynthetically active radiation (gray), nitrate (blue) and chlorophyll (green) measured during the HOT program (http://hahana.soest.hawaii.edu, station ALOHA, cruise 114; see also Karl 2010). Resource distributions plotted (a) on linear and (b) on logarithmic scales. As it is commonly supposed, the light intensity can be approximated by an exponential distribution (black dotted lines and R^2 values in (a) and (b)). In contrast, the nutrient profile exhibits two distinct regimes: In the area below the production layer the nutrient concentration can be well fit by a linear dependence ($R^2 = 0.91$, black dashed line in (a)); however, within the production layer an exponential distribution gives a better description ($R^2 = 0.99$, black dashed line in (b)). We argue that the regime of exponential decay within the production layer is more crucial for competition, because in this area growth can be nutrient limited, whereas in the linear part of the nutrient profile growth is nutrient saturated. Interestingly, the interval of exponential decay ranges over three orders of nitrate concentrations, making this area crucial for the competition among a wide range of phytoplankton species which can be limited by this nutrient (Litchman et al. 2007). Note, that similar exponential distributions in this interval of depths have been observed in mean nitrate concentrations between 1989-2006 (Karl & Letelier 2008). (c) System state curve (SSC), showing the distributions in the resource plane with logarithmic axes. The solid blue line shows actual cruise data for the light intensity and the nutrient. Since light intensities are not reported below a depth of 140 m, the system state curve was extrapolated, assuming that the light intensity follows the same exponential decay up to 300 m (blue dotted line). Dashed line shows a straight line fit (with R^2 value) within the production layer.

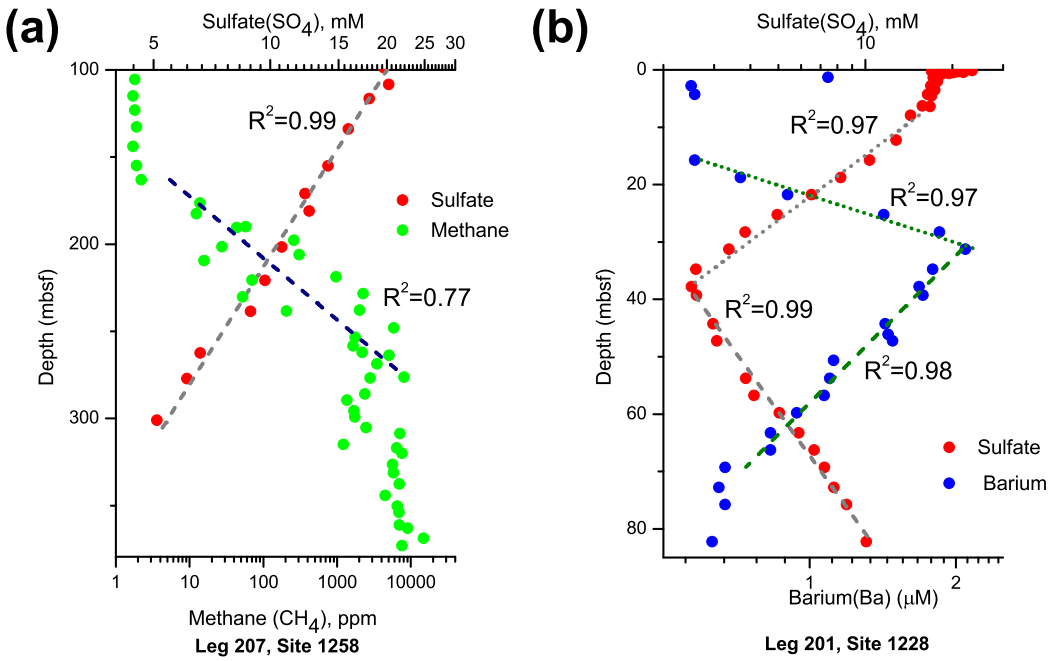

Figure S5: Exponential distribution of resource concentrations in deep marine sediments. Inverse concentration profiles (note the logarithmic scale) result from biologically catalyzed reactions, which consume and release metabolites in a complex biogeochemical reaction network deep in the sediment column.

(a) Concentration profiles of sulfate (red) and methane (green) from ODP leg 207, site 1258, Demerara Rise, Equatorial Atlantic (Shipboard Scientific party, 2004; Arndt et al. 2006) show a sulfate-methane transition zone in a sediment depth of 150-300 m. Substrates are supplied by a downward flux of sulfate from the sediment-water interface and by the biogenic production of methane from deeply buried organic matter in black shale sequences at a depth below 400 m. Upward diffusing methane and downward diffusing sulfate are depleted by deep sedimentary microbial communities in the process of anaerobic methane oxidation (AMO). Note that the exponential distribution of methane ranges over several orders of magnitude.

(b) Depth profiles of sulfate (red) and barium (blue) along the sediment column of ODP leg 201, site 1228, eastern Pacific ocean (Shipboard Scientific party, 2004; D'Hondt et al, 2004), exhibiting two reversed zonation patterns. The characteristic sulfate-barium transition zone that extends from the water-sediment interface to greater depth (0 to 40 m) is mirrored by a second reversed succession that extends upward from the basement-sediment interface in depth from 40 to 80 m. Here, sulfate enters the sediment from two directions: from the overlying ocean and from an underlying basaltic aquifer. In each transition zone the depletion of sulfate by microbial activity promotes the remobilization of biogenic barium (Torres et al. 1996), giving rise to high concentrations of dissolved barium in the pore fluids beyond the zone of sulfate depletion.

Data are obtained during the ocean drilling program (ODP, http://iodp.tamu.edu/). Dashed and dotted lines show straight line fits to the data on the logarithmic axes. R^2 values of the fit are indicated.

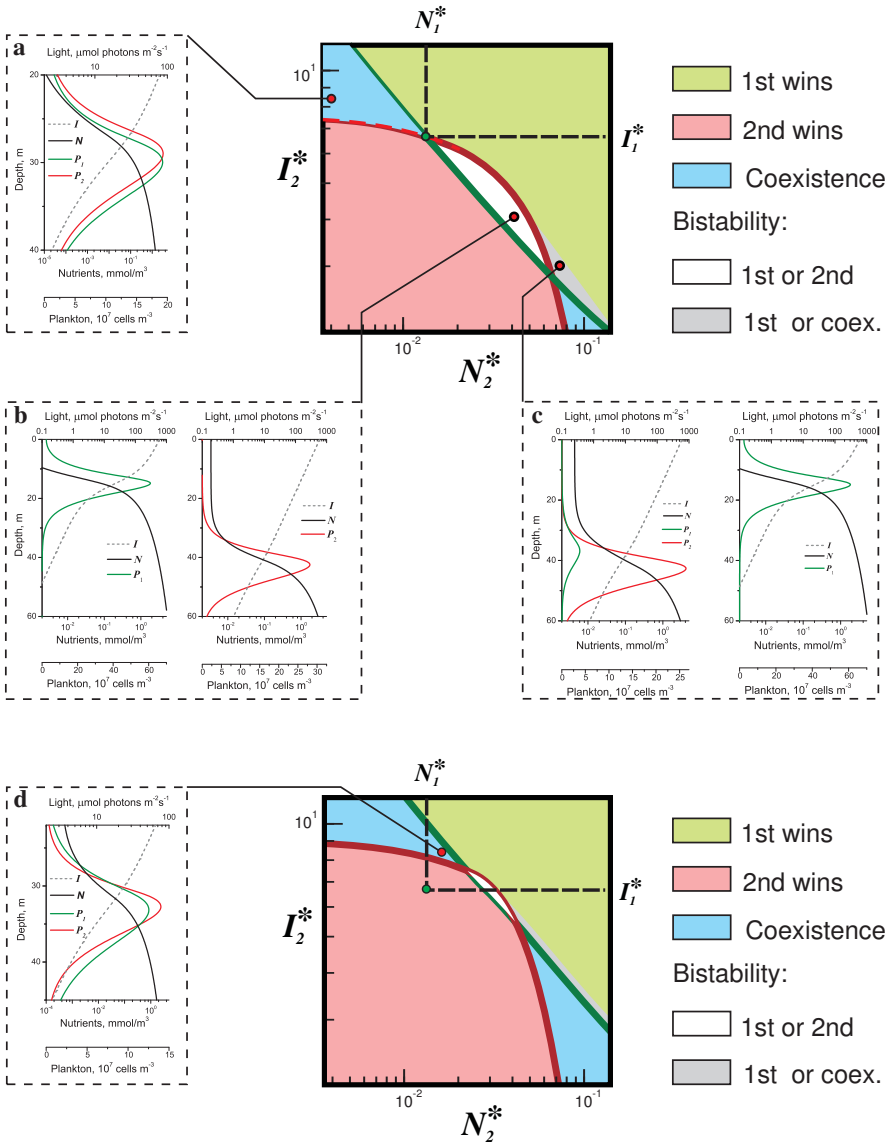

Figure S6: Illustration of different competition outcomes in the phytoplankton model. The outcome of two species competition is shown (indicated by color coding), depending on the critical resource values of species 2 (critical resources (N_1^*, I_1^*) of species 1 fixed, green circle), when the maximal growth rates and mortalities are identical (top panel), or differ by the factor $\beta = 2$ (bottom panel), similar to Fig. 5 from the main text. Insets (a) - (d) show typical spatial profiles corresponding to the different competition regimes (critical resource values of species 2 indicated as red circle). Plotted are the phytoplankton concentration of species 1 (green) and species 2 (red), and the distribution of light (black dashed line) and nutrient (black solid line) as a function of depth z.

(a) and (d): Two fundamentally different coexistence mechanisms in a spatial system. (a) Coexistence due to a resource limitation trade-off, mediated by niche segregation in resource requirements which becomes apparent as a spatial separation of density profiles. (d) Coexistence due to a gleaner-opportunist trade-off. The two species are not spatially separated, but species 1 with smaller resource requirements (gleaner) can utilize a larger favorable range, whereas the high growth rate of the stronger resource limited species 2 (opportunist) allows it to survive on a smaller spatial range.

(b) and (c): Two kinds of bistability in the competition outcome. (b) Alternative stable state when each species cannot grow in the presence of its competitor. (c) Alternative stable states of either coexistence (species 1 can invade the monoculture of species 2, but does not reach a high abundance) or a monoculture of species 1 (species 2 cannot establish in the presence of species 1).

Parameter values of species 1 see in Table S1. Simulation parameters for species 2: (a) $H_{I,2} = 24.7$ μmol photons m^{-2} s^{-1}, $H_{N,2} = 0.012$ mmol nutrient m^{-3}, (b) $H_{I,2} = 12.2$ μmol photons m^{-2} s^{-1}, $H_{N,2} = 0.123$ mmol nutrient m^{-3}, (c) $H_{I,2} = 9$ μmol photons m^{-2} s^{-1}, $H_{N,2} = 0.22$ mmol nutrient m^{-3}, (d) $H_{I,2} = 24.7$ μmol photons m^{-2} s^{-1}, $H_{N,2} = 0.044$ mmol nutrient m^{-3}.

Table S1: Default model parameters

Symbol	Interpretation	Units	Value
Independent variables			
t	Time	h	
z	Depth	m	
Dependent variables			
$P(z,t)$	Population density	cells m^{-3}	
$I(z,t)$	Light intensity	μmol photons m^{-2} s^{-1}	
$N(z,t)$	Nutrient concentration	mmol nutrient m^{-3}	
Parameters			
I_{in}	Incident light intensity	μmol photons m^{-2} s^{-1}	600 $(100 \dots 1000)^*$
K_{bg}	Background turbidity	m^{-1}	0.1 $(0.01 \dots 1)^*$
Z_B	Depth of the water column	m	100
D	Vertical turbulent diffusivity	cm^2 s^{-1}	0.3 $(0.01 \dots 0.7)^*$
N_B	Nutrient concentration at Z_B	mmol nutrient m^{-3}	10 $(0.1 \dots 10)^*$
Species 1			
H_I	half-saturation constant for light	μmol photons m^{-2} s^{-1}	20
H_N	half-saturation constant for nutrient	mmol nutrient m^{-3}	0.04
k	light attenuation coefficient	m^2 cell^{-1}	$6{\times}10^{-10}$ $(1{\times}10^{-10} \dots 1{\times}10^{-9})^*$
α	cell nutrient content	mmol nutrient cell^{-1}	$2{\times}10^{-10}$ $(1{\times}10^{-10} \dots 1{\times}10^{-9})^*$
$\mu_{\max}$	maximal growth rate	h^{-1}	0.04
m	mortality rate	h^{-1}	0.01
Species 2			
H_I	half-saturation constant for light	μmol photons m^{-2} s^{-1}	15
H_N	half-saturation constant for nutrient	mmol nutrient m^{-3}	0.065
k	light attenuation coefficient	m^2 cell^{-1}	$1{\times}10^{-10}$ $(1{\times}10^{-10} \dots 1{\times}10^{-9})^*$
α	cell nutrient content	mmol nutrient cell^{-1}	$5{\times}10^{-10}$ $(1{\times}10^{-10} \dots 1{\times}10^{-9})^*$
$\mu_{\max}$	maximal growth rate	h^{-1}	0.04
m	mortality rate	h^{-1}	0.01

* in Fig. 3b and Fig. S2.

Appendix S5 provides further details of simulation parameters specific to certain figures.